Investigation of particle-fluid interactions in a channel with the Lattice Boltzmann Method

Manxi (Maggie) Shi
BASIS Independent Silicon Valley, San Jose, CA 95131 manxishi@gmail.com

Abstract

Particle separation in a fluid has been studied in the past few decades since its early discovery. Particles in a channel focus at specific equilibrium radial positions, as they are subject to many fluid-induced and wall-induced lift and drag forces. The Lattice Boltzmann Method (LBM), developed recently, can handle particle-fluid interactions more conveniently than traditional CFD approaches like the finite difference or finite volume method based on the Navier-Stokes equations. In this work, we implement LBM in a Python code and investigate various boundary conditions to simulate Poiseuille flow and examine the interactions between a circular object and Poiseuille flow.

1 Introduction

The movement of particles in fluid microchannels is well studied for its applications in the pharmaceutical industry and biochemistry, including in particulate drug delivery [2], movement of cancer cells [3], and transfusion medicine [5]. Computational fluid dynamics is a powerful tool for modelling this and understanding flow-induced lift forces on particles in a microchannel [6] [7] [8] [1], which informs the development of advancements in diverse fields, from pharmaceuticals to circuit design. In this paper, the Lattice Boltzmann Method is used to model Poiseuille flow around a cylinder in a channel, a simplification of a particle in a microchannel.

The Lattice Boltzmann Method has grown in popularity in the last two decades as an alternative to traditional methods in computational fluid dynamics that are based on the Navier-Stokes equations. LBM takes a mesoscopic approach, looking at the fluid as a discrete particle distribution, as opposed to conventional methods that solve macroscopic partial differential equations, such as the finite difference and finite volume method.

Originating from the Lattice Gas Automata method (LGA) [10] [11] [17] and the Boltzmann equation in kinetic theory [14] [21], LBM has been popularized due to its ability to model problems involving complex boundary conditions, turbulence, and multiphase flow [18]. The main motivation behind the shift from LGA to LBM was to reduce statistical noise due to the nature of numerical calculation using an insufficient number of particles.

LBM is also considered as a special discretized form of the Boltzmann equation [25] because one can fully recover the Navier-Stokes equations under the assumption that density variation is small [24] with the Chapman-Enskog expansion.

An advantage of LBM over traditional Navier-Stokes CFD solvers is that communication is all local, so the algorithm can be parallelized to run on GPUs or high performance computers [19] [20].

This work analyzes various boundary conditions and presents simulations of Poiseuille flow and flow past a circular cylinder using the Lattice Boltzmann Method on a D2Q9 lattice. We also look into how cylinder radius affects the force on the cylinder. On the basis of these results, we can apply LBM to modelling processes involving the movement of a particle in a fluid channel, like aerosol particles depositing in lung airways.

Drug delivery for asthma and cystic fibrosis are often carried out through inhaled drugs, but many of these drug particles do not actually reach desired locations in the lungs, as particles deposit along the respiratory tract on the way. Fluid dynamical models modelling the movement of aerosol drug particles could inform the development of novel drug delivery methods or help scientists formulate improved inhaled drugs. CFD models can improve our understanding of how factors like pressure in the drug delivery canisters, drug particle size, and fluid temperature affect the movement of particles through airways and deposition on the channel walls [4].

2 Particle-Fluid Interaction

A particle in a fluid flow with variable velocity profile such as the parabolic velocity profile in Poiseuille flow experiences forces applied towards or away from the wall depending on size of the particle, distance to the wall, and velocity profile of the flow. There are three main mechanisms such force can arise.

1. When a particle is very close to the wall, the velocity of the fluid near the wall is close to zero due to the no-slip boundary condition. The velocity of the fluid on the side of the particle away from the wall is greater, and the streamlines of the flow are squeezed, leading to a smaller pressure on side facing the center of the channel. This is a typical Bernoulli setup where faster flow attaches to the round particle resulting in a low pressure. The pressure difference pushes the particle away from the wall (Figure 1).

   For a spherical object, an empirical equation is given (Di Carlo et al 2009, Gao et al 2017)

   $$F_{wall} = C_{wall}\rho U^2 \frac{D_p^6}{D^4} \tag{1}$$

   where C_{wall} is an empirical dimensionless wall induced lift coefficient, ρ is the fluid density, U is the maximum flow velocity, D_p is the particle diameter, and D is the channel diameter.

2. In the case where the flow profile is quadratic, the exact difference in velocity profile causes relative velocity difference as the particle flows with a mean velocity. The relative velocity on

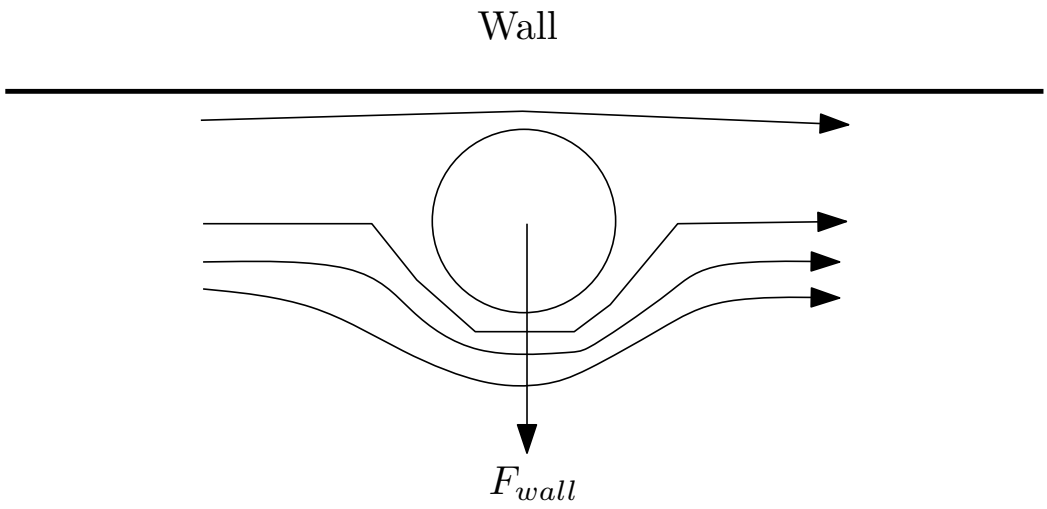

Figure 1: Flow squeeze away from the wall leads to a force away from the wall

the side away from the wall is smaller than the relative velocity on the side close to the wall. This results in a pressure difference and a net force towards the wall for particles anywhere in the channel (Figure 2).

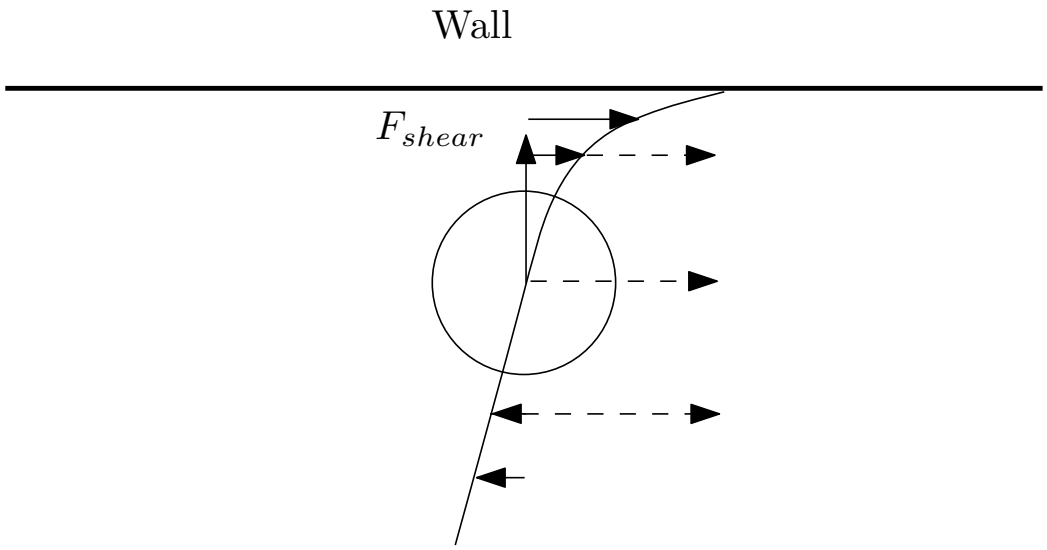

Figure 2: Quadratic velocity distribution leads to a force towards the wall

For a spherical object, an empirical equation is given (Di Carlo et al 2009, Gao et al 2017)

$$F_{shear} = C_{shear}\rho U^2 \frac{D_p^3}{D^4} \tag{2}$$

where C_{shear} is an empirical dimensionless shear induced lift coefficient, whose magnitude depends strongly on the Reynolds number and particle's radial position.

3. The rotation of a particle in a fluid gives rise to a third lift force, known as the Magnus effect. One half of a rotating spherical particle will increase the velocity of the fluid, resulting in a lower pressure area, according to Bernoulli's theorem. The other half decreases the velocity of the fluid, resulting in a higher pressure area. This pressure difference causes a force away from the wall (Figure 3).

   An equation estimating this rotation-induced lift force $F_{rotation}$ is given by Rubinow and Keller (1961)

$$F_{rotation} = \frac{1}{8}\pi D_p^3 \rho \omega \times \mathbf{V} \tag{3}$$

   where ω is the angular velocity vector and $\mathbf{V}$ is the relative velocity vector in fluid's rest frame. $F_{rotation}$ is negligible when particles are far from the walls, but near the wall, where the shear-induced force and wall-induced forces cancel each other, the rotation-induced force becomes relevant.

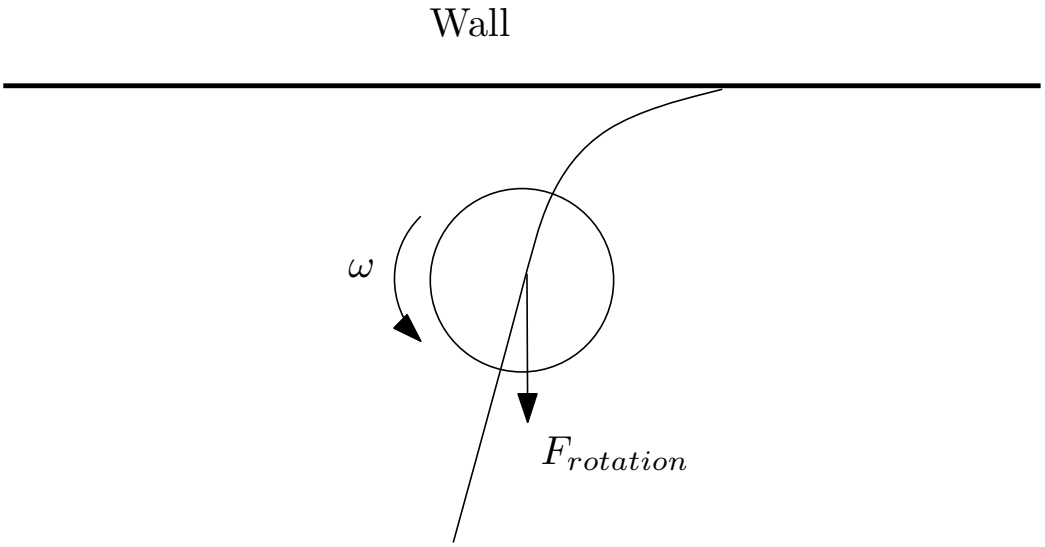

Figure 3: Rotation of the particle leads to a force away from the wall

Particles in channeled flow with a Poiseuille velocity profile interact with the flow in such a way that they are focused at equilibrium positions, as reported by Segré (1961). Due to the complexity of the interaction, theoretical studies cannot yield complete and satisfactory results describing the behavior of the particles. We investigate the interaction through numerical methods used in computational fluid dynamics.

3 The Lattice Boltzmann Model (LBM)

The Lattice Boltzmann Model is based on a discretized Boltzmann equation and models fluid as discrete particles moving on a lattice grid and colliding with other particles. LBM is divided into two main

steps: streaming and collision. Every particle is given a unit vector velocity, and during the streaming step, it is moved along its velocity direction to the next lattice node. The collision step describes the redistribution of particles at the node post-streaming.

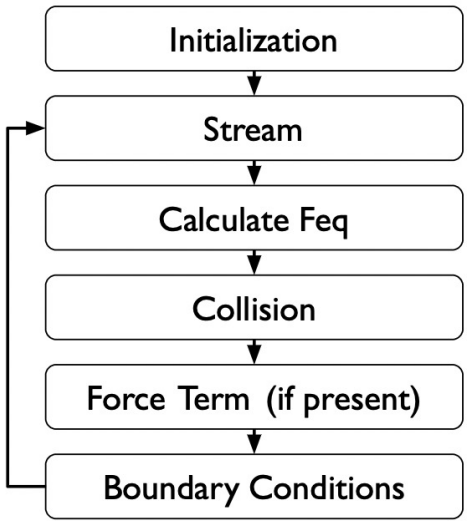

Figure 4: Algorithm flowchart

The most popular Lattice Boltzmann Model uses the Bhatnagar-Gross-Kook (BGK) approximation, which describes the relaxation of a non-equilibrium distribution to an equilibrium distribution. LBM models are typically implemented on a DnQm lattice, meaning n dimensions and m velocity directions. A 2D, 9-directional lattice was used, D2Q9 (Figure 5). A velocity unit vector $\mathbf{e_i}$ is assigned for each direction in the nine-velocity model. LBM can also be implemented in 3d, with D3Q15, D3Q19, and D3Q27 being the most common models.

The pressure-corrected equation governing the LBM, a discretized Boltzmann equation, proposed by Chen *et al.* [24] is

$$f_i(\mathbf{x}+\delta\mathbf{e_i},t+\delta) = \tilde{f}_i(\mathbf{x},t) = f_i(\mathbf{x},t)+\Omega_i[f(\mathbf{x},t)] \tag{4}$$

Where $f(\mathbf{x},t)$ is the pre-collision particle distribution, $\Omega_i[f(\mathbf{x},t)]$ is the collision operator using the BGK approximation, and $\bar{f}_i^i$ is the post-collision distribution function. $\bar{f}_i^i$ is streamed neighboring to neighboring nodes in the next step, becoming $f_i(\mathbf{x}+\delta\mathbf{e_i},t+\delta)$. The time step δ and lattice spacing Δx are chosen so that a particle travels one lattice spacing in one time step.

The particle distribution, $f_i(\mathbf{x},t)$, is the probability of finding a particle at position $\mathbf{x}$ at time t. The Boltzmann equation describes the propagation of particles as a contribution of two components: the streaming step and the collision step. The streaming step carries particles to neighboring nodes every time step. The collision step describes the interaction of particles at a node, producing a new distribution. Ω is the collision operator, given by the Bhatnagar-Gross-Kook approximation [26].

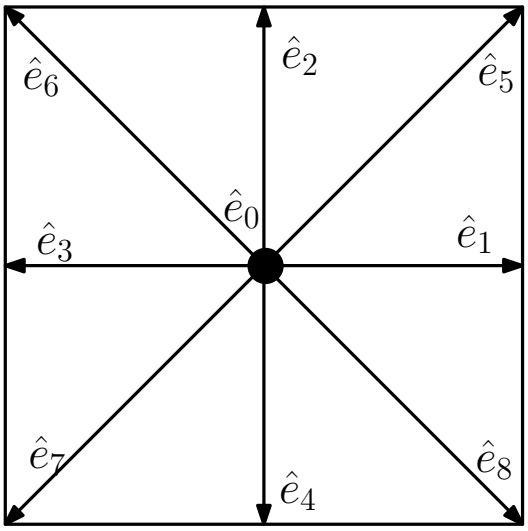

Figure 5: The commonly used D2Q9 LBM grid notation

$$\Omega_i(f) = -\frac{1}{\tau}\left(f_i(\mathbf{x},t) - f_i^{eq}(\mathbf{x},t)\right) \tag{5}$$

Ω is a function of the current distribution function and τ, the relaxation time, which describes the rate at which the distribution progresses to equilibrium. *tau* relates to the kinematic viscosity, ν, of the fluid as $\nu = \mathbf{c}^2(2\tau - 1)/2$, where $\mathbf{c}$ is the speed of a propagating wave in the fluid, $\mathbf{c}^2 = 1/3$.

The equation defining the equilibrium distribution for a D2Q9 lattice is given by

$$f_i^{eq} = \rho w_i \left[1 + 3\frac{\mathbf{e_i}\cdot\mathbf{u}}{\mathbf{c^2}} + 9\frac{(\mathbf{e_i}\cdot\mathbf{u})^2}{2\mathbf{c^4}} - 3\frac{\mathbf{u}^2}{2\mathbf{c^2}}\right] \tag{6}$$

where w_i are the predefined lattice weights based on the choice of the lattice and $\mathbf{u}$ is the velocity vector of the lattice.

D2Q9 lattice uses the following weights for the nine directions:

$$w_i = (4/9, 1/9, 1/9, 1/9, 1/9, 1/36, 1/36, 1/36, 1/36)$$

From the particle distribution, macroscopic density ρ and velocity $\mathbf{u}$ are described by the equations

$$\rho = \sum_i f_i \tag{7}$$

$$\mathbf{u} = \frac{1}{\rho}\sum_i f_i \mathbf{e_i} \tag{8}$$

Performing a Taylor expansion and using the Chapman-Enskog expansion, the Navier-Stokes equations describing macroscopic properties of the fluid can be recovered.

4 Boundary Conditions

No-slip condition is used as the boundary conditions in the LBM algorithm. An extrapolation scheme[13] was used for the top and bottom boundaries because of its second order accuracy. The common LBM bounce-back approach which is accurate in the first order was used at the boundary of the cylinder. Periodic boundary conditions were used at the inlet and outlet, effectively connecting the left and right end of the channel.

4.1 Periodic Boundary Conditions

Initially, periodic boundary conditions were used to perform a benchmark test of the accuracy of the LBM Python program with verified solutions and images of fluid flowing around a circular cylinder from other literature. Periodic boundary conditions streams fluid velocities from the top wall to the bottom wall and from the right outlet to the left inlet. Figure 5 shows the velocity grids at the four boundaries. After streaming, velocities in directions 1, 5, and 8 exiting the right boundary become velocities in directions 1, 5, and 8 entering the left boundary. Similarly, velocities in directions 2, 5, and 6 exiting the top boundary become velocities in directions 2, 5, and 6 entering the bottom boundary. Thus, periodic boundary conditions imply that the fluid section analyzed is a small section of an infinite expanse of fluid. Periodic boundary conditions were not used at the top and bottom walls because other methods were used to simulate the presence of walls. They were used at the inlet and outlet to simulate the scenario of a long tube.

Periodic boundary conditions are simply taken care of with NumPy's roll function.

4.2 Extrapolation Scheme

However, the objective of modelling fluid flow confined by walls cannot be achieved with periodic boundary conditions, so next, we look into the extrapolation scheme, a method to simulate the presence of no-slip wall boundaries.

The extrapolation method [13][30][31] is based off the idea of placing ghost nodes inside the walls, beyond the fluid and boundary. As shown in Figure 6, the subscript f describes a fluid node, b a boundary node, and w a ghost node inside the wall.

We decompose the distribution function into an equilibrium and non-equilibrium part.

$$f_i = f_i^{neq} + f_i^{eq}$$

For the lattice nodes the walls, instead of using (6) we approximate f_i^{eq} with the equation

$$\bar{f}_i^{eq} = \rho w_i \left[1 + 3\frac{\mathbf{e_i} \cdot \bar{\mathbf{u}_w}}{\mathbf{c^2}} + 9\frac{(\mathbf{e_i} \cdot \bar{\mathbf{u}_w})^2}{2\mathbf{c^4}} - 3\frac{\bar{\mathbf{u}_w}^2}{2\mathbf{c^2}} \right] \tag{9}$$

where $\bar{\rho}_w \approxeq \rho(\mathbf{x_f})$ approximates ρ_w and $\mathbf{u}_w$ is an approximation of the wall velocity to be chosen, depending on q.

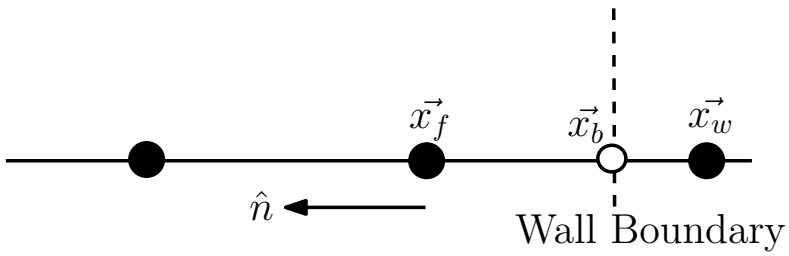

Figure 6: The extrapolation method for boundary condition, a ghost node is inserted at $\vec{x}_b = \vec{x}_w + h(1-q)\hat{n}$ [32] where h is the lattice length, $q \in (0,1]$ is adjustable ratio, and $\hat{n}$ is the unit vector from wall towards the fluid.

For $q \geq 0.75$, $\bar{\mathbf{u}}_w = \frac{\mathbf{u}_b + (q-1)\mathbf{u}_f}{q}$

For $q < 0.75$, $\bar{\mathbf{u}}_w = (q-1)\left(\mathbf{u}_f + \frac{1-q}{1+q}\mathbf{u}_{ff}\right)$

Following finding $\bar{f}_i^{eq}$, the algorithm carries on with calculating the post-collision distribution.

In our program, $q = 0.5$, and the extrapolation scheme was used at the top and bottom wall boundaries.

4.3 Bounce Back Approach

The bounce back approach [24] at the walls reverses the directions of incoming velocities. For example for the nodes at the top wall, velocities in directions 2, 5, and 6 are pointing into the wall (Figure 5). After applying bounce back boundary conditions, the particle distributions f_2, f_5, and f_6 become f_4, f_7, and f_8 and vice versa. The directions with a y velocity component are reversed, so that the resulting y velocity becomes opposite in direction.

This simple bounce-back approach was implemented at the cylinder boundaries.

5 Python Implementation

The LBM algorithm is implemented in a python code. The different steps of the algorithm are executed in sequence, initial condition, boundary condition, equilibrium state calculation (6), collision (5), and streaming (4). The loop boundary condition, equilibrium state calculation, collision update, and streaming is repeated until a desired end time is reached.

One subtlety of the LBM algorithm is the use of lattice units instead of physical units. The lattice units for mass, length and time can be converted to physical units and vice versa through conversion factors (Chapter 7 in [9])

The roll function in Python's NumPy library "rolls" values along an axis of an array. This made streaming update particularly easy to implement. In the program, a 3d array stored the particle densities in the nine directions for every lattice point, with the dimensions of the array being the x coordinate, y coordinate, and velocity direction. Using NumPy's roll function, the distribution functions in all

nine directions were rolled to the next node in the direction of the corresponding velocity during the streaming stage of the algorithm.

The Python program has integrated graphing utilities implemented so that the result of the simulated can be visualized conveniently. For Poiseuille flow, an x-velocity vs y-position plot was used to see the parabolic velocity profile. For flow around a cylinder, a color map of vorticity was used to see the Kármán vortex street develop at high Reynolds numbers and laminar flow at low Reynolds numbers.

6 Poiseuille Flow

Poiseuille flow is the laminar flow typically seen in a viscous, incompressible fluid flowing through a narrow channel. At equilibrium the velocity profile within the channel approaches a parabolic shape. Poiseuille flow modelled in 3d would have a similar velocity profile, with y and z velocities being zero. In this work, a 2d model was used to model a fluid flowing in the positive x direction, thus the velocity in the y direction is zero. Examples of Poiseuille flow include saline solution flowing through an IV tube and blood flowing in a capillary.

To achieve the parabolic velocity profile of Poiseuille flow, a uniform pressure gradient in the x direction, periodic boundary conditions at the inlet and outlet, and top and bottom walls were imposed.

Fluid tends to flow from high to low pressure, so a pressure gradient was imposed accordingly. A pressure gradient causes a force on the fluid at every node, so an additional term was added to the Boltzmann equation. The equilibrium state then becomes

$$f_i^{eq} = \rho w_i \left[1 + 3\frac{\mathbf{e_i} \cdot \mathbf{u}}{\mathbf{c^2}} + 9\frac{(\mathbf{e_i} \cdot \mathbf{u})^2}{2\mathbf{c^4}} - 3\frac{\mathbf{u}^2}{2\mathbf{c^2}} \right] + P_i \tag{10}$$

where P_i is the pressure gradient term added to the equilibrium state functions.

In addition to a constant pressure gradient, periodic boundary conditions at the inlet and outlet were used. Connecting the inlet and outlet simulate the situation of a long pipe. Poiseuille flow naturally develops in a long pipe over time, given a uniform initial x-velocity.

An extrapolation scheme was used at the top and bottom boundaries to simulate the presence of walls. Poiseuille flow develops a parabolic velocity profile because the fluid velocity at the walls is zero, due to a no-slip condition.

The analytical solution for Poiseuille flow is

$$u_x = \frac{\Delta P}{4\nu L}(H^2 - y^2)$$

where ΔP is the pressure difference between the inlet and outlet, ν is the kinematic viscosity, L is the channel length, H is the channel height, and y is the radial position.

For this LBM program, pressure differences on the order of magnitude 10^{-5} were used. Figure 7 shows the analytical solution g in red and the computational solution in blue.

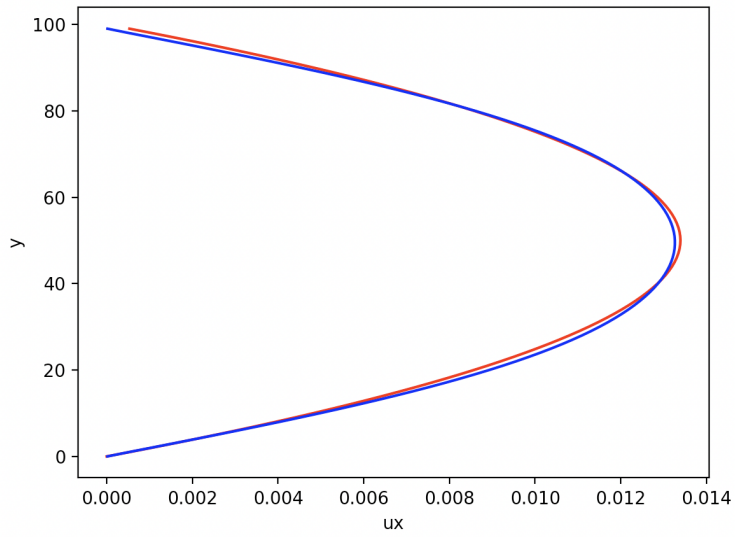

Figure 7: Parabolic velocity profile of Poiseuille flow

7 Flow around a Cylinder

Flow around a cylinder is a benchmark test of any fluid dynamics simulation. Typically, we plot a color map of vorticity or velocity to see the Kármán vortexes develop at high Reynolds numbers. In this work, the Re number was a parameter that then influenced τ, the relaxation time, and thus influences equilibrium particle distribution.

For low Reynolds numbers, the flow is laminar, in Figure 8. At around $Re = 170$, the streamline starts to wiggle a bit. For high Reynolds numbers, a Kármán vortex street develops, in Figure 9.

7.1 Flow-Induced Force on the Cylinder

Force on the particle can be found through the momentum exchange method. We can compute the momentum change of the neighboring particles in a straightforward manner in LBM because there are equations describing macroscopic velocity and density (7). The particle momentum is given as

$$p = \sum_i f_i \mathbf{e_i} \tag{11}$$

where i iterates through the 9 dimensions of the lattice grid. The momentum change of the particle before and after collision can be found

$$\Delta p = p_{after} - p_{before} = \sum_i (f_i \mathbf{e_i})_{after} - \sum_i (f_i \mathbf{e_i})_{before} \tag{12}$$

The impulse applied on the wall from the fluid is the opposite of the above momentum change. The momentum exchange method is easily implemented at the cylinder due to the simple bounce-back wall boundary condition.

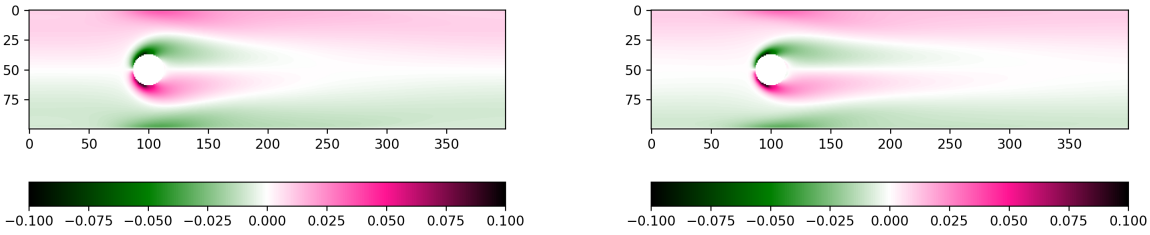

Figure 8: a) Re 60 b) Re 120

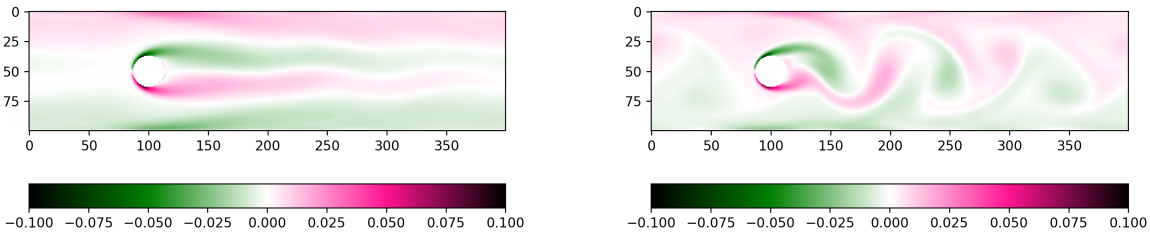

Figure 9: a) Re 180 b) Re 290

7.1.1 Drag and lift coefficients

Drag and lift coefficients can be calculated from the lift and drag forces with the equations[34]

$$C_d = \frac{2F_D}{\rho U^2 D}$$

$$C_l = \frac{2F_L}{\rho U^2 D}$$

where ρ is the average fluid density, U is the free stream velocity, and D is the diameter of the cylinder.

Plotting C_d and C_l over time produces oscillations, and with the vortex shedding oscillation frequency f_w, the Strouhal number is defined as

$$S_t = \frac{f_w D}{U}.$$

7.1.2 Force with varying cylinder sizes

The force on a cylinder increases linearly with cylinder radius. The R-squared value of 0.998 indicates a strong linear correlation. An increased number of particle collisions with the boundary explains the greater force, as the force is calculated as a sum of the momentum exchange (Figure 10).

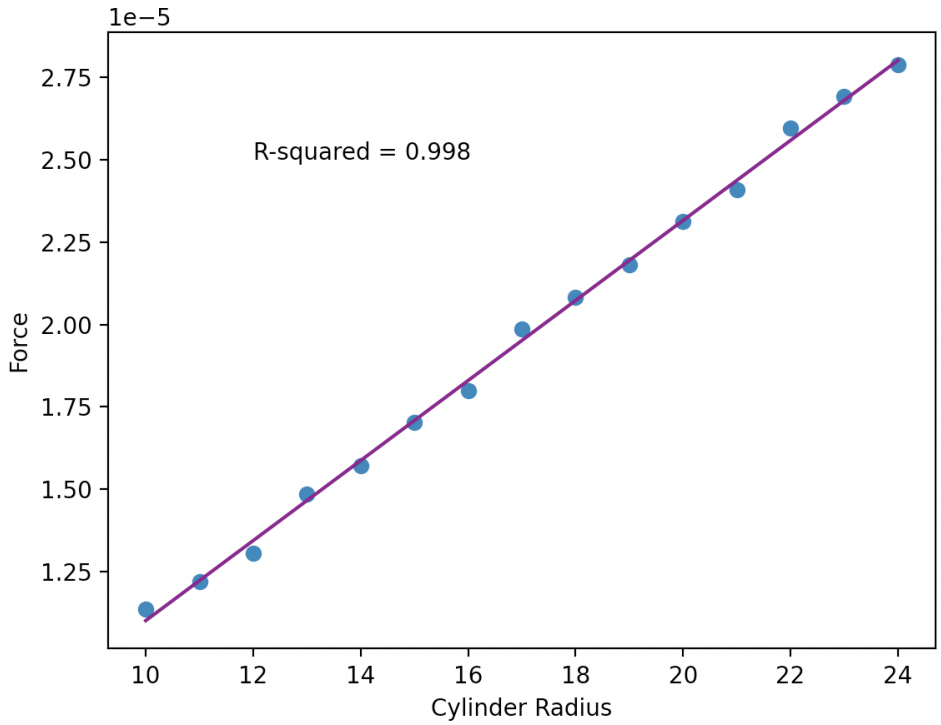

Figure 10: There is a strong linear correlation between the radius of the cylinder and the force on the cylinder.

7.1.3 Force with varying pressure gradients

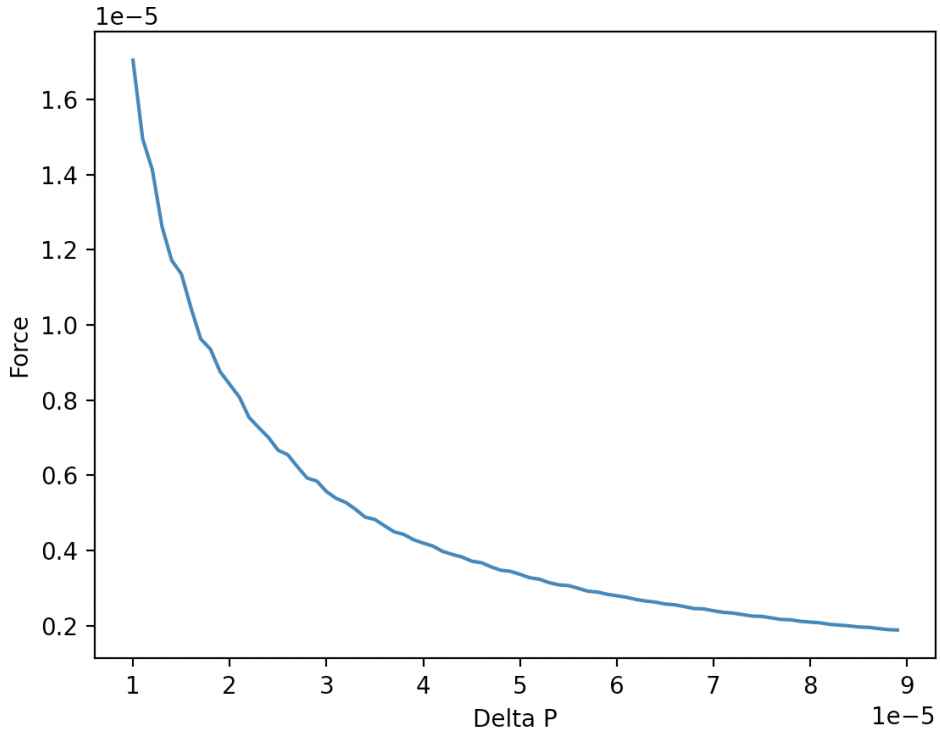

Figure 11: Increasing the pressure difference between the inlet and outlet of the channel leads to the force on the cylinder asymptotically decreasing.

Increasing the pressure difference between the inlet and outlet leads to faster fluid flow, which causes flow separation. Flow separation in flow around an obstacle is the detachment of the fluid boundary layer into a wake, resulting in reduced lift and an increased pressure-induced drag. This phenomenon is typically undesirable, which is why tennis balls have fuzz and golf balls have dimples. When the pressure difference is on the order of 10^{-5} lattice units, increasing ΔP decreases the force on the cylinder, explained by increased drag and reduced lift forces (Figure 11).

8 Results

The program simulating fluid flow with the Lattice Boltzmann method proved its accuracy with benchmark tests of Poiseuille flow and flow around a cylinder. Kármán vortices were produced when the Reynolds number exceeded 180. At lower Re numbers, flow was laminar. This work extends the model to include momentum change calculations to find the force on a cylinder placed in a fluid channel.

Results show that cylinder radius is positively and linearly correlated with the force experienced. Understanding the relation between particle size and force on a particle can benefit scientists designing

aerosol drugs, for example, because we can find an optimal particle size where delivery is controlled and efficient. Additionally, results show that increasing the pressure difference across the inlet and outlet of the channel causes the force on the cylinder to decrease asymptotically. This is a result of decreased lift forces and increased drag forces due to flow separation at high pressure differences.

9 Future Research

Parallelizing code for running on a GPU and programming in Fortran or C for faster computation is also a future research goal, as LBM's algorithm lends to easier parallelization, compared to traditional Navier-Stokes solvers. Extending this D2Q9 model to a D3Q19 model is also a possibility, to visualize the simulation in 3d.

Future research could involve applying this Lattice Boltzmann model to modelling the deposition of aerosol drug particles in airways. These particles flowing through airways are subject to the complex forces discussed in this work, and shear-induced forces cause particles to flow towards channel walls and deposit. When drug particles deposit on the walls on the way to reaching their intended destination, the drugs do not achieve their full strength. Creating fluid dynamical models of this phenomenon could help scientists design new aerosol drugs that are more efficient in their delivery. This would entail creating an LBM model where particle obstacles in the fluid channel can move in real time, influenced by the fluid around it. This can be achieved by calculating the force on every lattice of the boundary of the obstacle and updating the boundary lattice layer accordingly at every time step.

References

[1] Segré, G.; Silberberg, A. Radial Particle Displacements in Poiseuille Flow of Suspensions. Nature 1961, 189, 209–210.

[2] Di Carlo, D., Irimia, D., Tompkins, R. G., and Toner, M., 2007, "Continuous Inertial Focusing, Ordering, and Separation of Particles in Microchannels," Proc. Natl. Acad. Sci. U.S.A., 104(48), pp. 18892–18897.

[3] Saliba, A. E., Saias, L., Psychari, E., Minc, N., Simon, D., Bidard, F. C., Mathiot, C., Piergac, J., Salamero, V. J., Saada, V., Vielh, P., Malaquin, L., and Viov, J., 2010, "Microfluidic Sorting and Multimodal Typing of Cancer Cells in Self-Assembled Magnetic Arrays," Proc. Natl. Acad. Sci. U.S.A., 107(33), pp. 14524 –14529.

[4] Longest P.W., Bass K., Dutta R., Rani V., Thomas M.L., El-Achwah A., Hindle M. Use of computational fluid dynamics deposition modeling in respiratory drug delivery. Expert Opinion Drug Delivery. 2019 Jan16(1):7-26. Epub 2018 Dec 10. PMID: 30463458; PMCID: PMC6529297.

[5] Greve, B., Valet, G., Humpe, A., Tonn, T., and Cassens, U., 2004, "Flow Cytometry in Transfusion Medicine: Development, Strategies and Applications," Transfus. Med. Hemother., 31, pp. 152–61.

[6] Li, J.; Webb, C.; Pandiella, S.; Campbell, G. A Numerical Simulation of Separation of Crop Seeds by Screening—Effect of Particle Bed Depth. Food Bioprod. Process. 2002, 80, 109–117.

[7] Viduka, S.M.; Feng, Y.Q.; Hapgood, K.; Schwarz, M. Discrete particle simulation of solid separation in a jigging device. Int. J. Miner. Process. 2013, 123, 108–119.

[8] Trunk, R.; Weckerle, T.; Hafen, N.; Thäter, G.; Nirschl, H.; Krause, M.J. Revisiting the Homogenized Lattice Boltzmann Method with Applications on Particulate Flows. Computation 2021, 9, 11. https://doi.org/10.3390/computation9020011

[9] Kruger T., et al, The Lattice Bolzmann Method Principles and Practice, Springer Cham, 2017

[10] Mohamad, A. A. Lattice Boltzmann Method Fundamentals and Engineering Applications with Computer Codes, Springer, London, UK, 2011

[11] A. Wongcharoen and S. Kingkaew, Simulation of Stenosis in Blood Vessel by Lattice Boltzmann Method," 2018 Third International Conference on Engineering Science and Innovative Technology (ESIT), 2018, pp. 1-4, doi: 10.1109/ESIT.2018.8665200.

[12] Succi, Sauro. (2003). The Lattice Boltzmann Equation – For Fluid Dynamics and Beyond. 10.1016/S0997-7546(02)00005-5.

[13] Chen, S., Martínez, D., Mei, R. (1996). On boundary conditions in lattice Boltzmann methods. Physics of Fluids, 8(9), 2527–2536.

[14] Boltzmann, L. Lectures on Gas Theory; Courier Corporation: Chelmsford, MA, USA, 2012.

[15] Shan X., Chen H. Lattice Boltzmann model for simulating flows with multiple phases and components. Phys. Rev. E. 1993;47:1815–1819. doi: 10.1103/PhysRevE.47.1815

[16] Mohamad, A. A. Applied lattice Boltzmann method for transport phenomena, momentum, heat and mass transfer. Canadian Journal of Chemical Engineering, vol. 85, no. 6, Dec. 2007, p. 946. Gale Academic OneFile,

[17] Frisch U., Hasslacher B., Pomeau Y. Lattice Gas Automata for the Navier-Stokes Equation. Physical Review Letters, vol. 56, no. 14, April 1986, p. 1505.

[18] Parmigiani A., Huber C., Bachmann O., Chopard B. Pore-scale mass and reactant transport in multiphase porous media flows. Journal of Fluid Mechanics, vol. 686, 2011, p. 40-76. doi:10.1017/jfm.2011.268

[19] Dalcin L.D., Paz R.R., Kler P.A., Cosimo A., 2011. Parallel distributed computing using python, Adv. Water Resour., vol. 34, no. 9, p. 1124–1139.

[20] Schornbaum F. & Rüde U., 2016. Massively parallel algorithms for the lattice Boltzmann method on nonuniform grids, SIAM J. Scient. Comput., vol. 28, no. 2, p. 96–C126.

[21] Higuera F.J. & Jimenez J., 1989. Boltzmann approach to lattice gas simulations, EPL (Europhys. Lett.), vol. 9, no. 7, p. 663 doi:10.1209/0295-5075/9/7/009.

[22] Versteeg H.K., Malalasekera W., 2007. An Introduction to Computational Fluid Dynamics: The Finite Volume Method; Pearson Education: London, UK.

[23] Girault, V., Raviart P.A., Finite Element Methods for Navier-Stokes Equations, Springer Berlin, Heidelberg, 1986

[24] Chen, S., Wang, Z., Shan, X., Doolean, G. Lattice Boltzmann computational fluid dynamics in three dimensions. J Stat Phys 68, 379–400 (1992).

[25] Liu Y., 2012. A lattice Boltzmann model for blood flows, Applied Mathematical Modelling, vol. 36, no. 7, p. 2890-2899.

[26] P.L. Bhatnagar, E.P. Gross, M. Krook (1954). A Model for Collision Processes in Gases. I. Small Amplitude Processes in Charged and Neutral One-Component Systems. Physical Review. 94 (3): 511–525, 1954

[27] Boubakran M. & Mirzaee I., 2018. Numerical simulation of external flow around cylinder using improved lattice Boltzmann method. The Journal of Engineering, vol. 2018, no. 4, p. 248-253.

[28] Rubinow S, Keller JB (1961) The transverse force on a spinning sphere moving in a viscous fluid. Journal of Fluid Mechanics 11, 447-459.

[29] Di Carlo D, Edd JF, Humphry KJ, Stone HA, Toner M. Particle segregation and dynamics in confined flows. Phys Rev Lett. 2009 Mar 6;102(9):094503. doi: 10.1103/PhysRevLett.102.094503. Epub 2009 Mar 3. PMID: 19392526; PMCID: PMC4485430.

[30] Guo, Zhaoli & Zheng, Chuguang Shi, Baochang. (2002). An extrapolation method for boundary conditions in lattice Boltzmann method. Physics of Fluids. 14. 10.1063/1.1471914.

[31] Cheng-Hsien Lee, Zhenhua Huang & Yee-Meng Chiew. (2015). An extrapolation-based boundary treatment for using the lattice Boltzmann method to simulate fluid- particle interaction near a wall, Engineering Applications of Computational Fluid Mechanics, 9:1, 370-381, DOI: 10.1080/19942060.2015.1061554

[32] Maddu Shankar, S. Sundar. (2009). Asymptotic analysis of extrapolation boundary conditions for LBM. Computers Mathematics with Applications. Vol. 57, Issue 8, Pg. 1313-1323.

[33] Chen, Y., Cai, Q., Xia, Z., Wang, M. &; Chen, S. Momentum-exchange method in lattice Boltzmann simulations of particle-fluid interactions. Physical Review E 88, (2013).

[34] Kai Guo Xiongwei Cui Minghao Liu, 2018. "A Coupled Lattice Boltzmann-Volume Penalization for Flows Past Fixed Solid Obstacles with Local Mesh Refinement," Mathematical Problems in Engineering, Hindawi, vol. 2018, pg 1-12, January.